

# Probing Antiferroelectric-Ferroelectric Phase Transitions in $\text{PbZrO}_3$ Capacitors by Piezoresponse Force Microscopy

Haidong Lu, Sebastjan Glinsek, Pratyush Buragohain, Emmanuel Defay, Jorge Iñiguez, and Alexei Gruverman\*

Functional characterization of antiferroelectric (AFE) materials typically involves macroscopic testing of their nonlocal integrated information on their dielectric properties, such as polarization hysteresis loops, field-dependent strain, and capacitance while the local AFE properties have been rarely addressed. Here, a new protocol is demonstrated for local probing of the antiferroelectric/ferroelectric (AFE/FE) phase transition in  $\text{PbZrO}_3$  capacitors by piezoresponse force microscopy (PFM). PFM spectroscopy of the local AFE/FE phase transition parameters is performed and their spatial variability via two-dimensional mapping is investigated. It is shown that AFE hysteresis loops recorded by PFM in the bias-on regime exhibit four characteristic amplitude peaks. Within the framework of Landau theory, these features are attributed to a considerable increase in the electromechanical strain response due to the dielectric constant divergence during AFE/FE phase transitions. The proposed approach can be used to differentiate between the antiferroelectric and nonpolar dielectric phases in functional devices using the electrically induced polarization.

## 1. Introduction

Antiferroelectrics (AFE) comprise a group of electronic materials actively studied for their potential applications in high energy storage capacitors and power generators, high-strain transducers and actuators, pyroelectric and electrocaloric devices, to name just a few.<sup>[1–4]</sup> Their signature characteristic is a double hysteresis loop of the polarization versus an external electric field, resulting from an electrically induced transition from the nonpolar AFE state to the polar ferroelectric (FE) phase.<sup>[5–7]</sup> A microscopic picture for the AFE behavior proposed by Kittel<sup>[8]</sup> involves an antiparallel dipole alignment in adjacent subcells, which yields zero net polarization in the absence of an


electric field and no piezoelectric activity. Transition to the FE phase under the applied electric field is a result of dipoles aligning in one direction. The AFE/FE phase transition is accompanied by a sharp change in polarization, volume, electrooptic coefficients, dielectric constants, and strain,<sup>[4]</sup> furnishing these materials with rich functional properties. Although antiferroelectricity has been observed in rather diverse materials groups, such as liquid crystals and hydrogen-bonded compounds,<sup>[9–12]</sup> it is inorganic antiferroelectrics with perovskite structure that draw the greatest attention as the most promising for technological applications. In particular,  $\text{PbZrO}_3$ -based ceramics have been actively investigated since their properties could be effectively tailored through compositional, stoichiometric, and micro-

structural modification. Advances in the fabrication of the AFE films allowed significant enhancement of their functional properties through the improvement of their microstructure and opened a possibility for device downscaling.<sup>[13–16]</sup> The dielectric properties of the AFE materials have been extensively studied at the macroscopic level by measuring polarization and strain hysteresis loops and by recording transient currents during polarization switching.<sup>[3]</sup> These measurements employ macroscopic setups that collect the global integrated response from the entire device while information on the local AFE properties is missing. In the meantime, the development of miniaturized electronic devices requires a comprehensive understanding of the functional behavior at the micrometer scale level. Piezoresponse force microscopy (PFM) provides a valuable approach for conducting high-resolution studies of the static and dynamic properties of FE and other polar materials by taking advantage of their strong electromechanical coupling behavior.<sup>[17]</sup> It is natural to assume that, although the AFE materials do not show any electromechanical response in the absence of an external electric field, PFM could be readily applicable to the investigation of the AFE/FE transitions since these transformations are associated with a significant change in strain and, as such, exhibit characteristics of electromechanical coupling. Nevertheless, reports of the PFM studies of the AFE materials have been scarce so far.<sup>[18]</sup> Here, we report PFM studies of the switching behavior of the model AFE compound— $\text{PbZrO}_3$  (PZO). We show that the AFE hysteresis loops recorded by PFM in the PZO capacitors through the top electrode display characteristic peaks at the AFE/FE transition points. Consideration of

Dr. H. Lu, P. Buragohain, Prof. A. Gruverman  
Department of Physics and Astronomy  
University of Nebraska-Lincoln  
Lincoln, NE 68588-0299, USA  
E-mail: agruverman2@unl.edu

Dr. S. Glinsek, Dr. E. Defay, Prof. J. Iñiguez  
Materials Research and Technology Department  
Luxembourg Institute of Science and Technology  
Esch-sur-Alzette L-4362, Luxembourg

Prof. J. Iñiguez  
Department of Physics and Materials Science  
University of Luxembourg  
Luxembourg L-1511, Luxembourg

 The ORCID identification number(s) for the author(s) of this article can be found under <https://doi.org/10.1002/adfm.202003622>.

DOI: 10.1002/adfm.202003622

antiferroelectricity within the framework of Landau theory attributes these features to a considerable increase in the electromechanical strain response due to a near divergence of the dielectric constant during the AFE/FE phase transitions. Application of the PFM spectroscopic approach allows us to extract the local AFE/FE transition parameters, such as forward and backward switching voltages and provides a possibility of differentiating between the antiferroelectric and nonpolar dielectric phases in functional devices using the electrically induced polarization.

## 2. Results and Discussion

The PZO thin films used in this study have been grown by a chemical solution deposition (CSD) method on Pt-coated SiO<sub>2</sub>/Si substrates with a PbTiO<sub>3</sub> seed layer. A scanning electron microscopy (SEM) micrograph of the PbTiO<sub>3</sub> seed layer (Figure 1a) shows that the layer is not continuous, but consists of sub-100-nm nanoislands distributed over the Pt surface. The PZO films exhibit polycrystalline morphology with a lateral grain size in the 100–300 nm range (Figure 1b). Cross-sectional SEM imaging reveals that the grains extend through the whole film thickness (Figure 1c). X-ray diffraction (XRD) analysis reveals a single-phase perovskite phase with preferential out-of-plane (100)<sub>pc</sub> orientation (Figure 1d). Details of the sample preparation method can be found in the Experimental Section.

Representative results of the macroscopic characterization of the dielectric and electromechanical properties of the Pt/PbZrO<sub>3</sub>/Pt capacitors are shown in Figure 2a–c. A double

polarization–field (P–E) hysteresis loop in Figure 2a is a clear indication of their AFE behavior. Due to the underlying PbTiO<sub>3</sub> seed layer, there is a remanent polarization of 5.5 μC cm<sup>−2</sup> present at zero-field in the 60-nm-thick PZO capacitors. This value decreases with an increase in the PZO thickness yielding 1.5 μC cm<sup>−2</sup> for the 180-nm-thick PZO capacitors (Figure S1, Supporting Information). Quasi-static local strain loops measured by using an atomic force microscopy (AFM) system (Figure 2b) show a large strain change of about 0.7% at around 0.8 MV cm<sup>−1</sup>, i.e., at the fields associated with the AFE/FE transition. A strain derivative over the field yields a value of 20 pm V<sup>−1</sup> at zero field for the local effective piezoelectric coefficient *d*<sub>33</sub>. This relatively high value could be again attributed to the presence of the PbTiO<sub>3</sub> seed layer. The capacitance–field loops (Figure 2c) measured in the Pt/PZO/Pt capacitors show four peaks indicative of a significant capacitance signal enhancement at the AFE/FE transition. Local PFM spectroscopy measurements, carried out by monitoring the first harmonic electro-mechanical response to the AC modulation voltage applied to the tip superimposed on a sweeping DC voltage, produce the PFM amplitude hysteresis loops shown in Figure 2d.

Before we discuss the specific features of the measured hysteresis loops, particularly those obtained in PFM, it is useful to consider antiferroelectricity within the framework of Landau theory. The simplest Landau potential capturing AFE behavior, initially proposed by Kittel,<sup>[8]</sup> can be written as:

$$F = F_0 + 1/2\alpha A^2 + 1/4\beta A^4 + 1/2\alpha' P^2 + 1/4\beta' P^4 + 1/23\beta A^2 P^2 + g\eta A^2 + g'\eta P^2 + 1/2\gamma\eta^2 - EP \quad (1)$$

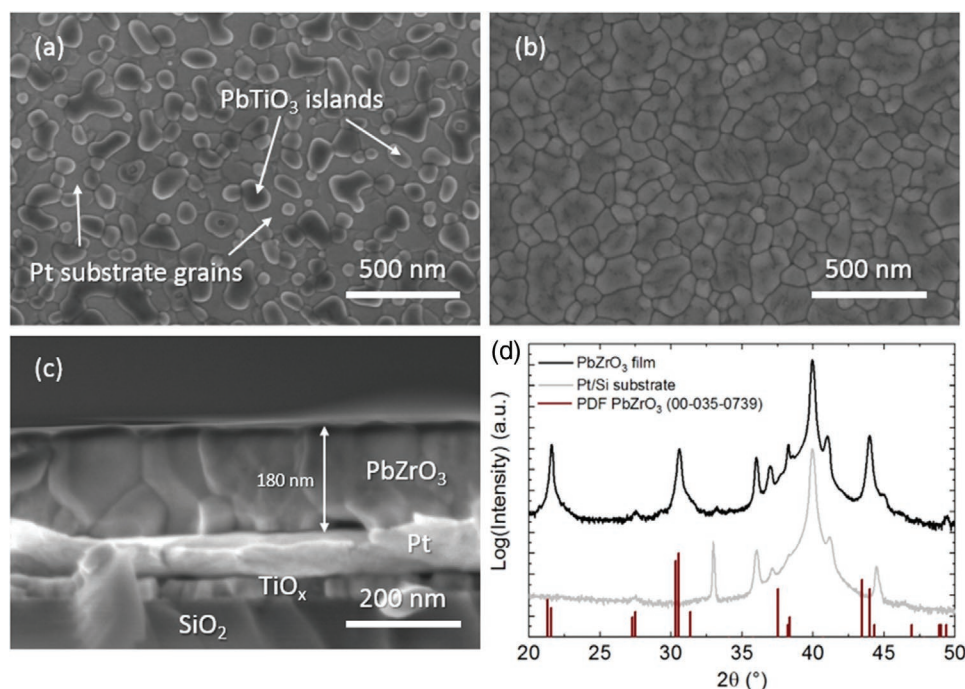


**Figure 1.** Structural characterization of the PbZrO<sub>3</sub> films. a,b) Scanning electron microscopy (SEM) micrographs of the PbTiO<sub>3</sub> seed layer on top of the Pt electrode (a), and the chemical solution deposition (CSD) grown 180-nm-thick PbZrO<sub>3</sub> film (b). c) SEM image of the cross-sectional view of the PbZrO<sub>3</sub> on top of the Pt/TiO<sub>x</sub>/SiO<sub>2</sub> substrate. d) X-ray diffraction (XRD) patterns of the PbZrO<sub>3</sub> film and Pt/Si substrate. Red vertical lines represent a randomly oriented P2cb phase.<sup>[28]</sup>

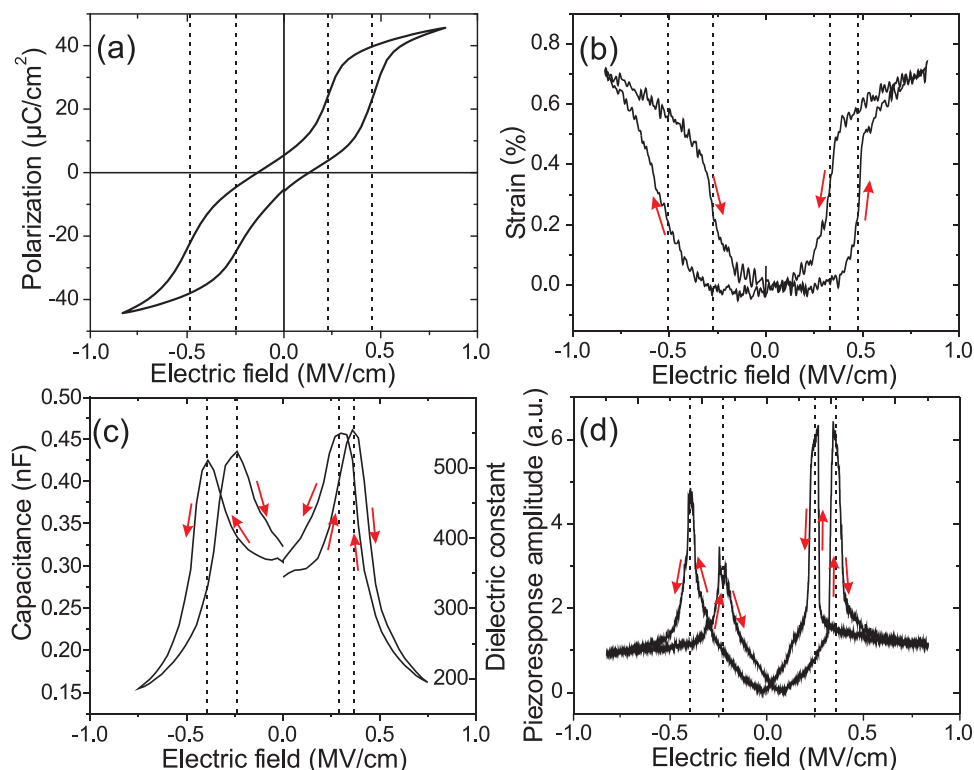


**Figure 2.** Electrical and electromechanical characterization of the 60-nm-thick Pt/PbZrO<sub>3</sub>/Pt capacitors. a) A polarization-field hysteresis loop measured at 1 kHz. b) A quasi-static strain-field hysteresis loop measured at 1 Hz using the AFM system. c) A capacitance-field loop with calculated dielectric constant at 1 mHz. d) A local piezoresponse force microscopy (PFM) amplitude loop. The vertical dashed lines indicate the antiferroelectric/ferroelectric (AFE/FE) transition fields, which vary from plot to plot due to the different measurement frequencies. Red arrows indicate the electric field sweeping directions.

where  $A$  and  $P$  are the AFE and FE order parameters, respectively, while  $\eta$  is the relevant (out-of-plane) strain, and  $\gamma > 0$  is the relevant elastic constant. As for the parameters controlling the energy, we have  $\alpha < \alpha' < 0$  and  $\beta > 0$ . The coupling with strain is given by  $g' < g < 0$ , so that the development of both  $A$  and  $P$  produces an elongation of the cell, the effect being stronger for the polarization  $P$ . The strain dependence on  $A$  and  $P$  can be expressed as:

$$\eta = -(1/\gamma)(gA^2 + g'P^2) \quad (2)$$

Based on this, it is possible to derive a strain-free potential with renormalized anharmonic couplings for  $A$  and  $P$ . This is the potential we assume in the following, disregarding the details of the renormalization as they are not essential.

Application of an electric field to an AFE sample will result in a linear increase of  $P$  and a quadratic decrease of  $A$ , up to the point when the AFE state stops being a minimum of the Landau potential, at which point the dielectric susceptibility will diverge. More specifically, it can be shown (see the Supporting Information for details) that the dielectric susceptibility is given by

$$\chi = [6\alpha + 8\beta A^2]^{-1} \quad (3)$$

so that  $\chi$  will become infinite when  $A^2 = -3\alpha/4\beta = 3/4 (A_0)^2$ , where  $A_0$  is the AFE order parameter at zero applied field. In other words, when the applied electric field reduces  $A$  to about

87% of its zero-field value, the system undergoes a transition to the polar FE state (AFE  $\rightarrow$  FE). The piezoelectric response is dominated by this singularity:

$$d\eta/dE \sim -(2/\gamma)(2gA_0 dA/dE + g'x^2)E \sim -(2/\gamma)g'x^2E \quad (4)$$

so that the PFM amplitude signal is zero at zero field and diverges together with the dielectric susceptibility. (Note that  $\gamma > 0$  and  $g' < 0$ , so that the piezoelectric response is always positive).

Discussion of the back transition to the AFE state upon the field reduction (FE  $\rightarrow$  AFE) follows a slightly different logic, since the Landau theory predicts the FE phase to be (meta)stable at zero field. The FE  $\rightarrow$  AFE transition occurs once the field is small enough so that (1) the AFE state is a minimum of the Landau potential (hence, the back-switching field must be smaller than the one at which the AFE  $\rightarrow$  FE transition occurs) and (2) the AFE state free energy is lower than that of the FE state. At the FE  $\rightarrow$  AFE transition, the polarization  $P$  reduces sharply going from a value of about  $(\alpha'/\beta)^{1/2}$  (corresponding to the spontaneous polarization  $P_0$  of the FE state) to nearly zero. The susceptibility of the FE state is given by  $\chi = (\alpha' + 3\beta P^2)^{-1}$  so that it will diverge at  $P^2 = 1/3 (P_0)^2$ , i.e., when  $P$  is reduced to about 58% of  $P_0$  as the FE  $\rightarrow$  AFE transition proceeds upon the field reduction. In this case, the piezoelectric response is given by:

$$d\eta/dE = -(2/\gamma)g'xP = -(2/\gamma)g'x(P_0 + xE) \quad (5)$$

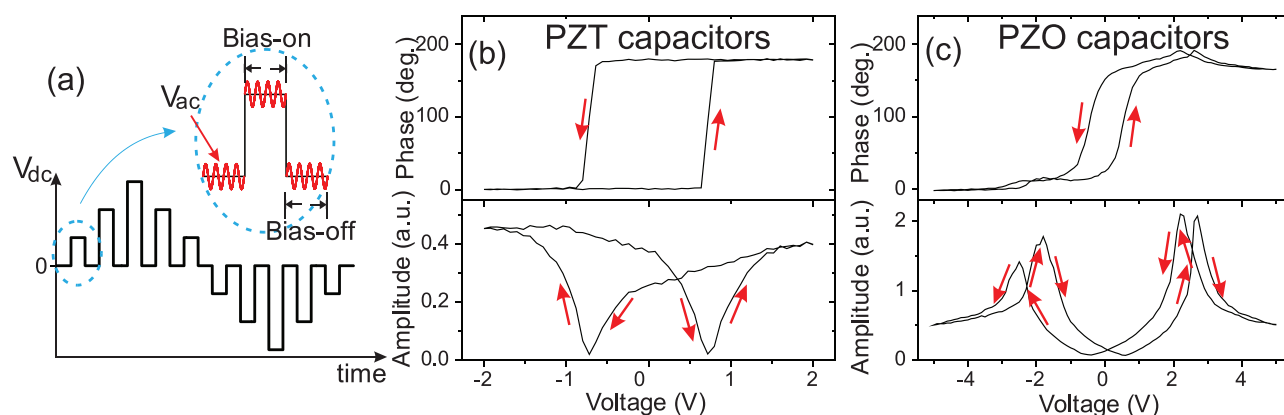


**Figure 3.** Comparative piezoresponse force microscopy (PFM) spectroscopy of the ferroelectric (FE) and antiferroelectric (AFE) capacitors. a) Pulsed triangular waveform with a superimposed small high-frequency AC bias for probing the PFM signal as a function of the switching DC bias. Inset illustrates a difference between the bias-on and bias-off regimes. b,c) Bias-on hysteresis loops measured in ferroelectric  $\text{Pb}(\text{Zr}_{0.4}\text{Ti}_{0.6})\text{O}_3$  (PZT) capacitors (b) and in antiferroelectric PZO capacitors (c). Top panels illustrate PFM phase loops and bottom panels show PFM amplitude loops. Red arrows indicate the electric field sweeping directions.

which is always positive ( $\gamma > 0$ ,  $g' < 0$ ) and non-zero even in the absence of the applied field and, again, diverges with  $\chi$ . Thus, the specific shape of the PFM amplitude hysteresis loops exhibited by the PZO capacitors in Figure 2c,d is a result of a drastic increase in the capacitive and electromechanical responses due to the sharp increase (in the ideal case, divergence) of the dielectric susceptibility of the PZO capacitors at the AFE/FE transition points.

It is important to discuss a difference in the PFM spectroscopy testing methodology of the FE and AFE capacitors. Conventional PFM spectroscopy employs a pulsed triangular waveform shown in Figure 3a with a superimposed high-frequency small AC bias for PFM signal detection.<sup>[19]</sup> The PFM loops can be acquired either when DC voltage is on (referred to as bias-on loops) or when it is off (bias-off loops). In the case of FEs, a choice for a specific PFM spectroscopy mode is made based on the experimental conditions and research goals. For example, bias-on loop measurements allow one to avoid polarization relaxation between pulses when no DC bias is present.<sup>[20]</sup> In contrast, bias-off measurements are recommended as a way to reduce the electrostatic contribution to the PFM signal when testing is done on a bare surface without a top electrode.<sup>[21]</sup> In any case, in PFM spectroscopy measurements, the FE capacitors typically exhibit a butterfly-type amplitude hysteresis loop irrespective of the spectroscopy mode used. Figure 3b shows the PFM bias-on hysteresis loops acquired from  $\text{Pb}(\text{Zr}_{0.4}\text{Ti}_{0.6})\text{O}_3$  (PZT) capacitors<sup>[22]</sup> where a finite PFM amplitude value at zero bias illustrates a stable remnant FE polarization while local minima in the PFM amplitude correspond to the balance between the antiparallel polarization states. These minima coincide with the  $180^\circ$  phase shift in the PFM phase loop manifesting a field-induced polarization reversal. The PFM loops measured in the PZT capacitors in the bias-off and bias-on regimes are compared in Figure S2 (Supporting Information). As expected, those loops show almost no difference.

In contrast, in the AFE materials, there is no net polarization in the absence of an external field, which means that PFM spectroscopy of these materials should be performed only in the bias-on regime. This, in turn, opens a possibility of PFM

probing of the field-induced AFE/FE transition. The PFM bias-on hysteresis loops measured in the AFE PZO capacitors shown in Figure 3c exhibit shapes that are drastically different from the PFM loops acquired from the PZT capacitors (Figure 3b): instead of two minima, the PFM bias-on amplitude loop features four maxima due to the divergence of the electromechanical signal at the AFE/FE transition as discussed above. The PFM bias-on phase loop exhibits a  $180^\circ$  difference between the signals for positive and negative voltages due to the field-induced FE states. The fact that the PFM phase signal is still detectable at zero bias can be explained by the presence of the thin FE  $\text{PbTiO}_3$  seed layer (which also results in a non-zero, albeit weak, PFM amplitude signal at zero field). In general, in a pure AFE sample, at zero bias the PFM amplitude signal should be negligibly small and the phase signal should become unstable. Note that in PFM spectroscopy of the FE or AFE capacitors, the hysteresis loops reflect the local electromechanical response even though the electric bias is applied to the entire capacitor volume. This provides a basis for a new protocol for evaluation of the local parameters of the AFE/FE transitions in the AFE structures, which is described below.

One of the greatest attributes of PFM is a possibility of an effective 2D mapping of the local physical characteristics of polar materials, such as nucleation bias, remnant polarization, and piezoelectric strain, which provides a nanoscale insight into the spatial variations of their properties. Switching spectroscopy PFM testing of the PZO capacitors has been carried out by point-by-point acquisition of the local hysteresis loops over a grid of  $32 \times 32$  points within the  $600 \times 600 \text{ nm}^2$  area. This provides a spatial resolution of about 20 nm, which is comparable with the PFM resolution for FE capacitors (about 25 nm) determined by the top electrode thickness.<sup>[23]</sup> Two examples of the individual PFM amplitude hysteresis loops (Figure 4a) taken at different locations clearly show point-to-point variations in the local transition voltages. Numerical analysis of the obtained loops allows extraction of the local AFE/FE transition parameters, which are shown in the form of 2D maps in Figure 4b–d: positive forward ( $V_{\text{pf}}$ ) and backward ( $V_{\text{pb}}$ ) biases corresponding to the  $\text{AFE} \rightarrow \text{FE}$  and  $\text{FE} \rightarrow \text{AFE}$  transitions in the positive voltage



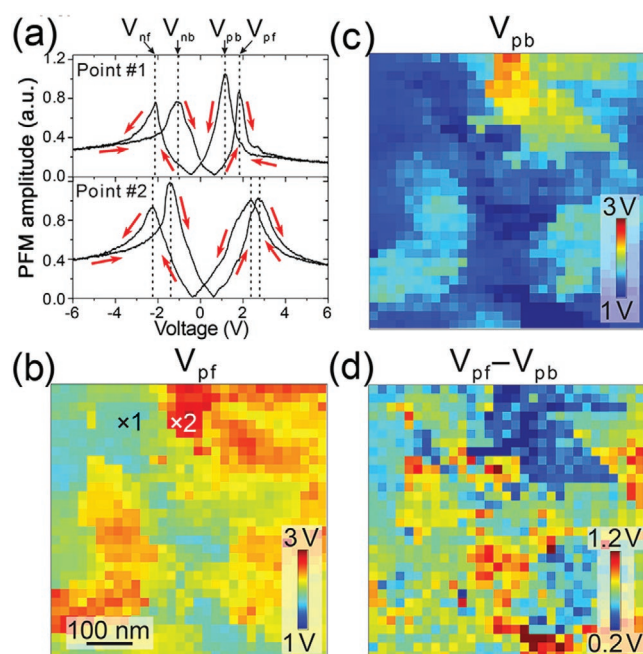


**Figure 4.** Piezoresponse force microscopy (PFM) switching spectroscopy of the 60-nm-thick  $\text{PbZrO}_3$  capacitors. a) Local PFM amplitude hysteresis loops acquired at points 1 and 2 marked in (b) illustrating the antiferroelectric/ferroelectric (AFE/FE) transition parameters, which are defined as voltages corresponding to the PFM signal peak values: positive forward bias  $V_{pf}$  – during the AFE  $\rightarrow$  FE transition with voltage increasing from 0 to 6 V; positive backward bias  $V_{pb}$  – during the FE  $\rightarrow$  AFE transition with voltage decreasing from 6 to 0 V; negative forward bias  $V_{nf}$  – during the AFE  $\rightarrow$  FE transition with voltage decreasing from 0 to -6 V; negative backward bias  $V_{nb}$  – during the FE  $\rightarrow$  AFE transition with voltage increasing from -6 to 0 V. b,c) 2D maps of the positive forward (b) and positive backward (c) voltages. d) 2D map of the loop width for the positive voltage range ( $V_{pf} - V_{pb}$ ). Red arrows indicate the electric field sweeping directions.

range, respectively, and a calculated loop width in the positive voltage range ( $V_{pf} - V_{pb}$ ). Variable colors of the maps illustrate significant nonuniformity of the AFE/FE transition voltages of up to 1.5 V within a distance of several tens of nanometers, likely reflecting the polycrystalline structure of the PZO capacitors. The AFE  $\rightarrow$  FE and FE  $\rightarrow$  AFE transition parameters for the negative voltage range are shown in Figure S3 (Supporting Information). The obtained results demonstrate the efficiency of PFM in testing the spatial variations of the local AFE properties and the parameters of the AFE/FE transitions.

### 3. Conclusion

In conclusion, we have applied PFM spectroscopy in the bias-on regime to probe the field-induced AFE/FE transitions in thin films of an archetype AFE material,  $\text{PbZrO}_3$ . We show that the PFM amplitude hysteresis loops acquired in the bias-on regime exhibit four characteristic amplitude peaks, which correspond to the field-induced AFE/FE phase transitions. More specifically, based on Landau theory consideration, these features could be attributed to a considerable increase in

the electromechanical strain response due to a near divergence of the dielectric constant at the AFE/FE transition points. We employed this bias-on PFM spectroscopy protocol to probe the uniformity of the local AFE/FE transition parameters, such as transition biases, loop width and strain, by acquiring 2D maps of these characteristics. The observed domain-like regions of about 200–300 nm in size with significantly different AFE/FE transition parameters reflect the polycrystalline structure of the PZO films. Importantly, this approach can be used to clarify a mechanism of the antiferroelectric-like behavior in the materials used in the functional devices using electrically controlled polarization. For example, the switching properties of the emerging FEs of the  $\text{HfO}_2$  family are often manifested by the pinched polarization hysteresis loops. Different schools of thought concurrently attribute this behavior either to the AFE or nonpolar dielectric constituent phases or strongly pinned FE domains.<sup>[24–26]</sup> Application of the proposed PFM spectroscopy approach opens a possibility to verify the presence of the AFE phase due to the unique signature features of its bias-on PFM amplitude hysteresis and investigate in detail the structural phase transformations induced by the AC cycling.

### 4. Experimental Section

**Thin Film Fabrication:** Based on the previously reported route,<sup>[27]</sup> the CSD method was used in this study. To prepare the  $\text{PbTiO}_3$  nucleation seed layer, a 0.1 M solution with initial composition of  $\text{Pb}_{1.3}\text{TiO}$  was spin-coated at 3000 rpm on platinized silicon (Pt/Si) substrates (Sintef, Norway) followed by drying and pyrolysis at 130 °C and 350 °C, respectively. Crystallization was performed at 700 °C in a rapid thermal annealing (RTA) furnace (AS-Master, Annealsys, France) in air. Due to low concentration of the  $\text{PbTiO}_3$  solution, the nucleation seed layer is not continuous and consists of nanoislands (Figure 1a). The  $\text{PbZrO}_3$  films were prepared by spin-coating a 0.3 M  $\text{PbZrO}_3$  solution with initial composition of  $\text{Pb}_{1.2}\text{ZrO}_3$  on the Pt/Si substrates with the  $\text{PbTiO}_3$  nucleation seed layer followed by a similar annealing process. The deposition–drying–pyrolysis steps were repeated several times before the crystallization to obtain the  $\text{PbZrO}_3$  films of a desired thickness. Thin films with the thickness of 60 and 180 nm were used in this study.

**Microstructural Characterization:** XRD patterns were recorded using  $\text{Cu-K}\alpha$  radiation in  $\theta$ - $2\theta$  geometry in a  $2\theta$  ranging from 20 to 50° with the step size and integration time of 0.02° and 2 s, respectively (D8 Discover, Bruker, USA). Surface and cross-sectional microstructures of the films were investigated using scanning electron microscope (SEM, Helios NanoLab 650, FEI, USA). Preferential out-of-plane (100)<sub>pc</sub> orientation of the  $\text{PbZrO}_3$  films is illustrated in Figure 1d by a relatively stronger intensity of the peaks at 21.6° and 43.9° in comparison with the randomly oriented films.

**Macroscopic Electrical Characterization:** The 100-nm-thick dc-sputtered Pt top electrodes with surface areas in the range between 25 and 40 000  $\mu\text{m}^2$  were patterned by lift-off photolithography. The fabricated Pt/ $\text{PbZrO}_3$ /Pt capacitors were tested using a commercial FE tester TF Analyzer 2000 E (aixACCT, Germany). For the PFM studies the Pt electrodes were 50-nm-thick.

**Piezoresponse Force Microscopy Measurements:** The PFM spectroscopy loops were measured using a commercial AFM system (MFP-3D, Asylum Research) using single crystal diamond probes (D80, K-Tek Nanotechnology). DC sweeping voltages at a frequency of 1 Hz with a superimposed high-frequency AC modulation signal (350 kHz, 0.3 V) were applied through the external electrical probe in contact with the deposited Pt top electrode. The AFM cantilever arm was also biased at the same potential as the top electrode to reduce the electrostatic interactions. The PFM spectroscopy imaging was done by measuring

the PFM hysteresis loops at each pixel of a  $32 \times 32$  matrix in a  $600 \times 600 \text{ nm}^2$  area.

**Quasi-Static Strain Loop Measurements:** The quasi-static strain loops were measured using the same AFM system by recording the static deflection signal of the AFM cantilever induced by sweeping a triangular-shaped voltage across the capacitor at 1 Hz. The deflection signal was then converted to the actual displacement in nanometers by taking into account the cantilever optical lever sensitivity. To obtain a strain value, the measured displacement was divided by the film thickness.

## Supporting Information

Supporting Information is available from the Wiley Online Library or from the author.

## Acknowledgements

The research at the University of Nebraska (H.L., P.B., and A.G.) was supported by the National Science Foundation (NSF) grant DMR-1709237 and through the Nebraska Materials Research Science and Engineering Center (MRSEC, grant DMR-1420645). S.G., J.L., and E.D. would like to thank Luxembourg National Research Fund for financial support (projects INTER/ANR/16/11562984/EXPAND/Kreisel and C16/MS/11348912/BIAFET). Drs. Aymen Mahjoub and Stéphanie Girod (Luxembourg Institute of Science and Technology) are acknowledged for their help with fabrication of capacitor structures.

## Conflict of Interest

The authors declare no conflict of interest.

## Keywords

antiferroelectricity, Landau theory, lead zirconate, phase transition, piezoresponse force microscopy

Received: April 25, 2020

Revised: June 11, 2020

Published online:

- [1] A. S. Mischenko, Q. Zhang, J. F. Scott, R. W. Whatmore, N. D. Mathur, *Science* **2006**, 311, 1270.
- [2] J. Parui, S. B. Krupanidhi, *Phys. Status Solidi* **2008**, 2, 230.
- [3] Z. Liu, T. Lu, J. Ye, G. Wang, X. Dong, R. Withers, Y. Liu, *Adv. Mater. Technol.* **2018**, 3, 1800111.
- [4] X. Hao, J. Zhai, L. B. Kong, Z. Xu, *Prog. Mater. Sci.* **2014**, 63, 1.
- [5] E. Sawaguchi, H. Maniwa, S. Hoshino, *Phys. Rev.* **1951**, 83, 1078.
- [6] E. Sawaguchi, T. Kittaka, *J. Phys. Soc. Jpn.* **1952**, 7, 336.
- [7] L. E. Cross, *J. Phys. Soc. Jpn.* **1967**, 23, 77.
- [8] C. Kittel, *Phys. Rev.* **1951**, 82, 729.
- [9] J. Lasave, S. Koval, N. S. Dalal, R. L. Migoni, *Phys. Rev. Lett.* **2007**, 98, 267601.
- [10] A. Fukuda, Y. Takanishi, T. Isozaki, K. Ishikawa, H. Takezoe, *J. Mater. Chem.* **1994**, 4, 997.
- [11] H. Takezoe, E. Gorecka, M. Cepic, *Rev. Mod. Phys.* **2010**, 82, 897.
- [12] X. Tan, C. Ma, J. Frederick, S. Beckman, K. G. Webber, *J. Am. Ceram. Soc.* **2011**, 94, 4091.
- [13] J. F. Li, D. D. Viehland, T. Tani, C. D. E. Lakeman, D. A. Payne, *J. Appl. Phys.* **1994**, 75, 442.
- [14] I. Kanno, S. Hayashi, M. Kitagawa, R. Takayama, T. Hirao, *Appl. Phys. Lett.* **1995**, 66, 145.
- [15] X. H. Hao, J. W. Zhai, X. Yao, *J. Am. Ceram. Soc.* **2009**, 92, 1133.
- [16] F. Wang, W. K. Li, G. H. Haertling, *Opt. Lett.* **1992**, 17, 1122.
- [17] A. Gruverman, M. Alexe, D. Meier, *Nat. Commun.* **2019**, 10, 1661.
- [18] K. Boldyreva, D. Bao, G. Le Rhun, L. Pintilie, M. Alexe, D. Hesse, *J. Appl. Phys.* **2007**, 102, 044111.
- [19] S. Jesse, A. P. Baddorf, S. V. Kalinin, *Appl. Phys. Lett.* **2006**, 88, 062908.
- [20] M. Alexe, A. Gruverman, Eds, *Ferroelectrics at Nanoscale: Scanning Probe Microscopy Approach*, Springer-Verlag, Berlin Heidelberg **2004**.
- [21] N. Balke, S. Jesse, Q. Li, P. Maksymovych, M. B. Okatan, E. Strelcov, A. Tselev, S. V. Kalinin, *J. Appl. Phys.* **2015**, 118, 072013.
- [22] A. Gruverman, B. J. Rodriguez, A. I. Kingon, R. J. Nemanich, J. S. Cross, M. Tsukada, *Appl. Phys. Lett.* **2003**, 82, 3071.
- [23] S. V. Kalinin, B. J. Rodriguez, S. H. Kim, S. K. Hong, A. Gruverman, E. A. Eliseev, *Appl. Phys. Lett.* **2008**, 92, 152906.
- [24] T. Schenk, E. Yurchuk, S. Mueller, U. Schroeder, S. Starschich, U. Böttger, T. Mikolajick, *Appl. Phys. Rev.* **2014**, 1, 041103.
- [25] T. Schenk, U. Schroeder, M. Pešić, M. Popovici, Y. V. Pershin, T. Mikolajick, *ACS Appl. Mater. Interfaces* **2014**, 6, 19744.
- [26] P. Buragohain, C. Richter, T. Schenk, H. Lu, T. Mikolajick, U. Schroeder, A. Gruverman, *Appl. Phys. Lett.* **2018**, 112, 222901.
- [27] N. Godard, S. Glinsek, E. Defay, *J. Alloys Compd.* **2019**, 783, 801.
- [28] S. Gates-Rector, T. Blanton, *Powder Diffr.* **2019**, 34, 352.